Molecular Biology of the Cell
Vol. 11, 2373–2385, July 2000

The Kar3p Kinesin-related Protein Forms a Novel Heterodimeric Structure with Its Associated Protein Cik1p

Jennifer G. Barrett, Brendan D. Manning, and Michael Snyder*

Department of Molecular, Cellular and Developmental Biology, Yale University, New Haven, Connecticut 06520-8103

Submitted January 19, 2000; Revised March 31, 2000; Accepted April 10, 2000
Monitoring Editor: Pam Silver

Proteins that physically associate with members of the kinesin superfamily are critical for the functional diversity observed for these microtubule motor proteins. However, quaternary structures of complexes between kinesins and kinesin-associated proteins are poorly defined. We have analyzed the nature of the interaction between the Kar3 motor protein, a minus-end–directed kinesin from yeast, and its associated protein Cik1. Extraction experiments demonstrate that Kar3p and Cik1p are tightly associated. Mapping of the interaction domains of the two proteins by two-hybrid analyses indicates that Kar3p and Cik1p associate in a highly specific manner along the lengths of their respective coiled-coil domains. Sucrose gradient velocity centrifugation and gel filtration experiments were used to determine the size of the Kar3-Cik1 complex from both mating pheromone-treated cells and vegetatively growing cells. These experiments predict a size for this complex that is consistent with that of a heterodimer containing one Kar3p subunit and one Cik1p subunit. Finally, immunoprecipitation of epitope-tagged and untagged proteins confirms that only one subunit of Kar3p and Cik1p are present in the Kar3-Cik1 complex. These findings demonstrate that the Kar3-Cik1 complex has a novel heterodimeric structure not observed previously for kinesin complexes.

INTRODUCTION

Microtubules are involved in a wide variety of cellular processes, including chromosome segregation, organelle and vesicle transport, and cell motility. The activities of two classes of microtubule motor proteins, the kinesins and dyneins, underlie these microtubule functions (reviewed by Hirokawa, 1998; Goldstein and Philip, 1999). Defining how microtubule motors assemble into functional complexes is crucial to understanding the molecular basis of their role in microtubule-mediated events.

Conventional kinesin is a complex of proteins identified by its role in anterograde axonal transport (Brady, 1985; Vale *et al.*, 1985). This heterotetrameric complex consists of two kinesin heavy chains (KHCs) and two associated proteins referred to as kinesin light chains (KLCs) (Bloom *et al.*, 1988; Kuznetsov *et al.*, 1988). KHC contains a microtubule-stimulated adenosine triphosphatase motor domain at its amino terminus (Scholey *et al.*, 1989; Yang *et al.*, 1990), a central coiled-coil stalk domain required for dimerization (deCuevas *et al.*, 1992), and a carboxy-terminal tail domain (Yang *et al.*, 1989). The carboxy-terminal region of the coiled-coil stalk and the amino-terminal portion of the tail domain of KHC form the binding site for KLCs (Gauger and Goldstein, 1993; Diefenbach *et al.*, 1998; Verhey *et al.*, 1998). The KLCs and the tail domain are thought to mediate kinesin binding to cargo (Skoufias *et al.*, 1994; Stenoien and Brady, 1997) and/or to regulate microtubule motor activity (Hackney *et al.*, 1992; Verhey *et al.*, 1998; Coy *et al.*, 1999; Friedman and Vale, 1999; Stock *et al.*, 1999). This structural organization is critical for the proper function of the kinesin complex.

The kinesin superfamily is a large ubiquitous family of proteins that share a region of homology with the motor domain of conventional KHC. These kinesin-related proteins (KRPs) are involved in a wide array of cellular processes (reviewed by Vale and Fletterick, 1997; Hirokawa, 1998; Goldstein and Philip, 1999). Consistent with their diverse functions, KRPs are structurally distinct from one another. Most members of the kinesin family, including conventional KHC, have amino-terminal motor domains and move toward the plus ends of microtubules. Members of the KIN I family have motor domains positioned internally relative to their primary sequence; the directionality and motor activity of these KRPs remain unclear (Desai *et al.*, 1999). Several KRPs, such as ncd (McDonald *et al.*, 1990), have motor domains at their carboxy termini and possess minus-end–directed motility. The nonmotor regions of the

* Corresponding author. E-mail address: michael.snyder@yale.edu.

majority of KRPs identified have stretches of primary sequence predicted to form α-helical coiled-coil interactions. However, aside from this structural feature, KRPs are highly divergent outside of their motor domains.

Considerable attention has been devoted to the identification of new KRPs and the mechanism by which the conserved motor domain moves along microtubules. However, less effort has been made to characterize kinesin-associated proteins (KAPs) that interact with nonmotor domains and that are likely involved in controlling the functional specificity of each KRP. Additionally, the quaternary structures of distinct KRP complexes are poorly defined. The few KRP complexes that have been characterized have diverse structures (reviewed by Vale and Fletterick, 1997; Hirokawa, 1998). As noted above, kinesin is a heterotetramer of two heavy chains and two light chains. BimC family members assemble into a bipolar homotetrameric complex containing two motor domains at each end of the structure (Kashina *et al.*, 1996; Gordon and Roof, 1999). Kinesin-II/Kif3 complexes form heterotrimers consisting of two distinct but related motor subunits that associate through a coiled-coil interaction and a single KAP that binds the tail domain of the complex (Cole *et al.*, 1993; Scholey, 1996; Wedaman *et al.*, 1996; Yamazaki *et al.*, 1996). As illustrated by these complexes, characterization of the diverse structural features of each KRP complex is important in defining the functional nature of each kinesin family member.

Kar3 is one of six *Saccharomyces cerevisiae* KRPs. It is essential for nuclear fusion during mating (karyogamy) and has distinct mitotic functions during vegetative growth (Meluh and Rose, 1990; Saunders and Hoyt, 1992; Saunders *et al.*, 1997; Cottingham *et al.*, 1999; Manning *et al.*, 1999). The Kar3 protein contains a motor domain at its carboxy terminus that possesses minus-end–directed motility and microtubule-depolymerizing activity (Meluh and Rose, 1990; Endow *et al.*, 1994). The nonmotor domain of Kar3p has a predicted α-helical coiled-coil domain of ~300 amino acids and an amino-terminal globular domain. This amino-terminal domain has a putative microtubule-binding site, because fusion proteins lacking the motor domain still localize to microtubules in vivo (Meluh and Rose, 1990; Page *et al.*, 1994). This domain structure of Kar3p could allow it to cross-link and slide microtubules relative to each other.

Kar3 interacts separately with two different KAPs, Cik1p and Vik1p (Page and Snyder, 1992; Page *et al.*, 1994; Manning *et al.*, 1999). Immunolocalization and genetic analyses have demonstrated that these Kar3p-associated proteins participate in distinct Kar3p-mediated processes, possibly by targeting the motor to different sites within the cell (Page *et al.*, 1994; Manning *et al.*, 1999). Cik1p is present in both vegetatively growing cells and cells treated with mating pheromone, whereas Vik1p is present only in vegetative cells. Cik1p and Vik1p are homologous proteins, but they share only 24% amino acid sequence identity over their entire lengths. However, they each have a centrally located 300-amino acid sequence predicted to form α-helical coiled-coil interactions. The existence of two novel KAPs that interact with this multifunctional KRP suggested that the Kar3p complexes might have a novel quaternary structure.

We have investigated the structure of the Kar3-Cik1 complex with the use of molecular genetic and biochemical approaches. We found that Kar3p and Cik1p form a tight complex through highly specific interactions over the entire lengths of their coiled-coil domains. Sizing and immunoprecipitation experiments demonstrate that the Kar3-Cik1 complex has a heterodimeric structure not observed previously for KRP complexes. The functional implications of this structure are discussed.

Table 1. Yeast strain list

Y864	*MATa ade2-101 trp1-901 leu2-3,112 ura3-52 his3-Δ200 gal4Δ gal80Δ plexAlacZ::URA3*
Y1700	*MATa ura3-52 lys2-801 ade2-101 trp1-Δ1 his3-Δ200 kar3Δ::TRP1*
Y1849	Y864 *cik1Δ::TRP1*
Y1850	*MAT a trp1-Δ1 his3-Δ200 leu2-Δ98 ura3-52 CANs cik1Δ::LEU2*
Y1861	*MATa his3-Δ200 ura3-52 leu2-Δ98 canR*
Y1870	Y1861 *KAR3::HAT*
Y1874	Y1870 *cik1Δ::LEU2*
Y2160	Y1861 *CIK1::HAT*

MATERIALS AND METHODS

Strains, Microbiological Techniques, and Two-Hybrid Analyses

Yeast strains used in this study are listed in Table 1. Unless stated otherwise below, other yeast strains have been described previously (Page *et al.*, 1994; Manning *et al.*, 1999). Manipulations and growth conditions were as described (Sherman *et al.*, 1986). Yeast transformations were performed with the use of lithium-acetate protocols (Ito *et al.*, 1983; Chen *et al.*, 1992).

Yeast two-hybrid techniques, including colony color assays and liquid β-galactosidase assays, were performed as described previously (Page *et al.*, 1994; Sheu *et al.*, 1998). Plasmids for these experiments were introduced into strains Y864 and Y1849. β-Galactosidase activities of Y864 strains containing two-hybrid plasmids with vector alone, *CIK1::lexA-DBD* constructs, and/or *KAR3::GAL4-AD* constructs were quantitated. Briefly, lysates from strains grown to midlogarithmic phase in plasmid-selective medium were incubated with o-nitrophenyl-β-D-galactopyranoside. The catalysis of o-nitrophenyl-β-D-galactopyranoside (assayed by spectrophotometry), the protein concentration of the lysates (measured with the use of a Bradford assay [Pierce, Rockford, IL]), and the amount of time required to produce the reaction were used to calculate the relative β-galactosidase activities.

Yeast Two-Hybrid Constructs

Molecular cloning techniques were performed as described previously (Sambrook *et al.*, 1989). *CIK1(20–541)::DBD* and *KAR3(12–514)::AD* have been described by Page *et al.* (1994). The *CIK1* two-hybrid constructs were made by either subcloning fragments of *CIK1* from a Bluescript vector (pSK*CIK1*) (Page and Snyder, 1992) or by PCR with this plasmid as a template. Fusions with the LexA DNA-binding domain (DBD) were made by cloning into the previously described pSH2-1 (Brent and Ptashne, 1985). *CIK1(20–169)::DBD* was made by ligating the *CIK1 Xho*I–*Sph*I fragment of pSK*CIK1* into the *Eco*RI site of pSH2-1. *CIK1(77–207)::DBD* was made by ligating the *CIK1 Ppu*MI–*Hpa*I fragment into the *Bam*HI site of pSH2-1. *CIK1(20–114)::DBD* was made by ligating the *CIK1 Xho*I–*Bst*NI fragment into the pSH2-1 *Eco*RI site. *CIK1(20–130)::DBD* was made by ligating a PCR fragment amplified with the use of primers JB17 (5′-GGATCCCGCTTTGACTTTTG-CATCTAATTCT-3′) and JB27 (5′-CGGGGATCCGAATGAATA-ACTCCAAAATTCCT-3′, which begins at the *CIK1*-coding sequence)

and digested with *Xho*I and *Bam*HI into the pSH2-1 *Eco*RI site. *CIK1(20–147)::DBD* was made by ligating a PCR fragment amplified with the use of primers JB18 (5′-GGATCCGTCCATCTCCGTTGATAGTCCATCA-3′) and JB27 and was digested with *Xho*I and *Bam*HI into the *Eco*RI site. *CIK1(77–169)::DBD* was made by ligating the *CIK1 Ppu*MI–*Sph*I fragment into the pSH2-1 *Bam*HI site. *CIK1(207–368)::DBD* was made by ligating the *Hpa*I–*Eae*I fragment into the *Eco*RI site. *CIK1(218–393)::DBD* was made by digesting pSK*CIK1* with *Eco*RI and ligating into the pSH2-1 *Eco*RI site.

CIK1(1–594)::AD, *KAR3(104–236)::AD*, *KAR3(176–294)::AD*, and *KAR3(238–408)::AD* were all cloned into pACTII (from S. Elledge, Baylor College of Medicine, Houston TX) with the use of PCR products amplified with primers designed to introduce restriction sites at the 5′ and 3′ ends. For instance, *CIK1(1–594)::AD* was made from a PCR fragment made with the primers JB28 (5′-CGGGGATCCTTTGTTTTGGCATTTGAAACTC-3′) and JB29 (5′-CGGGATCCTTAATCTAGCTGAGGTAATGT-3′), digested with *Bam*HI, and cloned into the *Bam*HI site of the pACTII vector.

The *SPA2::DBD* construct was described previously (Sheu *et al.*, 1998). The *KIP2::DBD* construct was made by PCR amplifying the entire *KIP2* ORF and cloning the resulting fragment into the *Nco*I–*Bam*HI site of pAS1-CYH2. All two-hybrid constructs were sequenced and remade or gap repaired if mistakes were detected.

Construction of Yeast Strains Containing Epitope-tagged Kar3p and Cik1p

A yeast strain with a fully functional genomic *KAR3::HAT* allele encoding Kar3p fused to three copies of the hemagglutinin (HA) epitope (Y1870) was made by means of a transposon insertional-tagging method (Ross-MacDonald *et al.*, 1997) and has been described (Manning *et al.*, 1999). A strain containing a fully functional genomic *CIK1::HAT* allele encoding Cik1p tagged with three copies of the HA epitope (Y2160) within its amino-terminal globular domain was prepared with the use of the same transposon insertional-tagging method (Ross-MacDonald *et al.*, 1997). The functionality of this fusion allele was determined by its ability to complement all *cik1*Δ phenotypes (Page and Snyder, 1992); this strain grows similar to isogenic wild-type strains at all temperatures, has normal microtubule structures, and does not display defects in mating.

Immunoprecipitations and Immunoblots

For the immunoprecipitation experiments shown in Figures 1 and 6, lysates were prepared from mating pheromone-treated cells. Cells were grown on yeast extract, peptone, adenine, and dextrose (YPAD) or synthetic complete medium lacking uracil for plasmid selection to an OD_{600} of 0.5–0.8. Ten OD_{600} units of cells were collected by centrifugation, resuspended in 15 ml of YPAD containing 5 μg/ml α-factor, and incubated for 2 h at room temperature (>80% of cells formed mating projections). Pheromone-treated cells were then harvested and lysed at 4°C in 100 μl of lysis buffer (100 mM NaCl, 10 mM EDTA, 2 mM EGTA, 5% glycerol, 40 mM Tris-HCl, pH 7.5, containing 1 μl of yeast protease inhibitor cocktail [Sigma Chemical, St. Louis, MO] and 200 μM PMSF) with the use of zirconia/silica beads (Biospec Products, Bartlesville, OK) and 40-s pulses of vortexing repeated six times. Samples were centrifuged for 10 min at 6500 × *g*, and 10 μl of lysate was removed for immunoblot analysis.

For immunoprecipitations, the lysates and beads were washed with 500 μl of lysis buffer containing detergents (1% NP-40, 0.5% sodium deoxycholate, and 0.1% SDS) at 4°C with rotation for 15 min. However, for extraction experiments (see Figure 1), lysates and beads were washed in this manner with 100 μl of lysis buffer containing 0.1, 2, or 4 M NaCl, 2 or 4 M urea, or 2% SDS. Samples were then centrifuged for 10 min at 6500 × *g*, and lysates were removed and diluted to a final volume of 1 ml with lysis buffer containing detergents. Cell lysates were precleared for 1 h with 40 μl of 50% slurry of protein A/G–agarose (Pierce) in lysis buffer. Precleared lysates were incubated with 5 μl of mouse monoclonal anti-HA antibodies (12CA5, BABCO, Richmond, CA) for 2 h with rotation, and protein-antibody complexes were then precipitated for 1 h with 40 μl of 50% slurry of protein A/G–agarose. Immunoprecipitates were collected by centrifugation at 2000 × *g* for 30 s, and pellets were resuspended in 1 ml of TBS (50 mM Tris, pH 8.0, 150 mM NaCl) containing detergents (1% NP-40, 0.5% sodium deoxycholate, and 0.1% SDS) and protease inhibitors (1 μl of protease inhibitor cocktail and 200 μM PMSF) and transferred to a fresh tube. Pellets were washed once more with 1 ml of TBS containing detergents and once with 1 ml of TBS before final resuspension in 30 μl of 2× Laemmli sample buffer (Laemmli, 1970).

For the vegetative immunoprecipitations, cells were grown as described above to an OD_{600} of 0.5–0.8, and 10 OD_{600} units of cells were collected by centrifugation. Cell lysates were prepared at 4°C in 100 μl of TBS containing protease inhibitors (1 μg/ml leupeptin, 1 μg/ml pepstatin, 2 μg/ml aprotinin, 100 μM chymostatin, 100 μM antipain, and 200 μM PMSF) with the use of acid-washed glass beads (Sigma Chemical) and vortexing as described above. Lysates and beads were washed briefly by vortexing for 20 s with 500 μl of TBS containing 0.5% SDS. Samples were then centrifuged for 20 min at 14,000 × *g*, and lysates were removed and subjected to immunoprecipitation as described above. Anti-Cik1p immunoprecipitations were performed by 5 h of incubation with 10 μl of rabbit polyclonal anti-Cik1p antibodies (Page and Snyder, 1992).

Proteins from cell lysates, immunoprecipitations, sucrose gradient fractions, and gel filtration fractions were detected by SDS-PAGE and immunoblot analysis with mouse monoclonal anti-HA antibodies (16B12, BABCO), rabbit polyclonal anti-Cik1p antibodies (Page and Snyder, 1992), or rabbit polyclonal anti-Kar3p antibodies (Meluh and Rose, 1990) as described previously (Manning *et al.*, 1999).

Sucrose Gradient Velocity Sedimentation

To prepare lysates for sucrose gradient velocity centrifugation, 25 ml of cells were grown to an OD_{600} of 0.5, pelleted, washed, and resuspended in 200 μl of PBS ($KHPO_4$, pH 8.0, 140 mM NaCl) plus protease inhibitors (PBS+) in a 5-ml borosilicate glass tube. Acid-washed glass beads were added up to the meniscus, and the tube was vortexed at 4°C six times for 30 s each (>90% of cells lysed). A total of 200 μl of PBS+ was added to the lysate, and the lysate was vortexed briefly and centrifuged at 14,000 × *g* for 20 min to clear cell debris. The cleared lysate was then filtered in a 0.2-μm syringe-top filter (Millipore, Bedford, MA), added to standards, and loaded onto the top of a 5-ml 5–20% linear sucrose gradient made with PBS+. Gradients were spun at 35,000 rpm at 4°C for 20 h in an SW 55-Ti rotor (Beckman Instruments, Fullerton, CA). Fractions (~275 μl) were collected dropwise into 1.7-ml Eppendorf tubes prepared with fresh protease inhibitors. Aliquots were added to 5× Laemmli buffer and boiled, and proteins were separated via SDS-PAGE. Two sets of gels were run for each experiment: one was stained with Coomassie brilliant blue to determine the fractionation of protein standards, and the other was immunoblotted with anti-Cik1p (Page and Snyder, 1992) and anti-HA (16B12, BABCO) antibodies. Immunoblots from wild-type experiments were cut between the known sizes of Cik1p and Kar3-HATp before antibody incubation so that the same blots were analyzed for both. Proteins present on immunoblots were quantified with the use of NIH Image software (version 1.59). Sedimentation values were determined by comparing the mobilities of Cik1p and Kar3-HATp with linear plots of the mobilities of standards: catalase, molecular mass = 250 kDa, 11.3S; aldolase, molecular mass = 158 kDa, 7.35S; BSA, molecular mass = 66 kDa, 4.4S. Peak fractions from three experiments were pooled and run on a gel filtration column.

Gel Filtration

Fractions corresponding to the slower-sedimenting Cik1p peak, the faster-sedimenting Cik1p/Kar3-HATp peak, or the single vegeta-

tive Cik1p peak were pooled, filtered, added to protein standards, and loaded onto a Sephacryl S-300 high-resolution gel filtration column and run via fast protein liquid chromatography (FPLC; Pharmacia, Piscataway, NJ) with PBS at 0.5 ml/min. A UV monitor was used to determine the void volume and total volume of the run. One-milliliter fractions were collected, added to 5× Laemmli buffer, and boiled. Proteins were then separated via SDS-PAGE and either stained for protein standards or immunoblotted as described above. The Stokes radius (Rs) of Cik1p was calculated by the method described by Cole *et al.* (1994). The average mobility of the protein (K_{av}) was calculated as: (volume eluted − void volume)/(total volume − void volume). Plots of Rs versus $-\log_{10} K_{av}1/2$ gave linear plots that allowed the determination of the Rs for Cik1p. This Rs value and the sedimentation coefficient were used to calculate the apparent molecular mass of the Kar3p-Cik1p complex with the use of the Svedberg equation (Cantor and Schimmel, 1980).

RESULTS

Cik1p and Kar3p Form a Stable Complex

To analyze the structure of the Kar3p-Cik1p complex, we used cells treated with the α-factor mating pheromone. Pheromone-treated cells were used for several reasons. First, previous studies have shown that Cik1p coimmunoprecipitates with Kar3p when extracts made with these cells are used (Page *et al.*, 1994). Second, the expression of both *KAR3* and *CIK1* is induced ~20-fold in cells incubated in the presence of mating pheromone relative to vegetative cells (Meluh and Rose, 1990; Page and Snyder, 1992). Finally, Cik1p is the only known Kar3p-associated protein in pheromone-treated cells (Manning *et al.*, 1999).

We first investigated the stability of the Kar3p-Cik1p complex in cell lysates from a *KAR3-HAT* strain. This strain encodes a fully functional version of Kar3p containing a 93-amino acid 3XHA/transposon (HAT) insertion at Ser^{68} of the Kar3p amino-terminal globular domain (Manning *et al.*, 1999). Lysates from *KAR3-HAT* cells treated with α-factor were prepared, incubated for 15 min in the presence of 0.1, 1, or 2 M NaCl, 1 or 2 M urea, or 1% SDS, and then diluted 10-fold. Kar3-HATp was immunoprecipitated from these lysates with the use of anti-HA antibodies, and the presence of Kar3-HATp and Cik1p was detected by immunoblot analysis. Cik1p remains associated with Kar3p even after treatment with up to 2 M NaCl or 2 M urea (Figure 1). As expected, the presence of 1% SDS disrupted the Kar3p-Cik1p complex, and neither protein was detected in anti-HA immunoprecipitations from a *KAR3* untagged strain. Thus, Kar3p and Cik1p form a tightly associated complex.

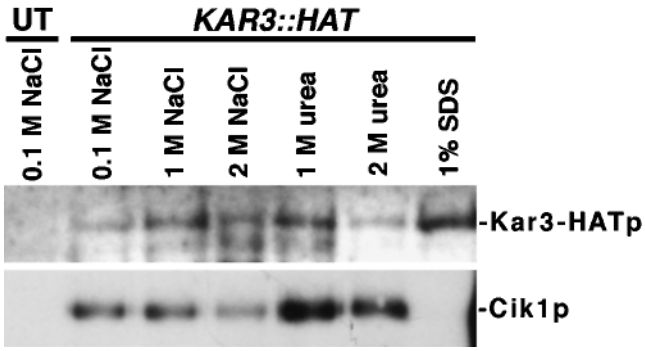

Figure 1. Kar3p and Cik1p are tightly associated. Lysates from an untagged strain (Y1861; UT) or a *KAR3::HAT* strain (Y1870) were treated with final concentrations of 0.1, 1, or 2 M NaCl, 1 or 2 M urea, or 1% SDS. Lysates were then diluted and immunoprecipitated with anti-HA antibodies. Immunoblot analysis with anti-HA antibodies (top blot) and anti-Cik1p antibodies (bottom blot) were used to detect coimmunoprecipitation of Kar3-HATp and Cik1p from these treated lysates.

Cik1p and Kar3p Interact in a Specific Manner Throughout Their Coiled-Coil Domains

A previous study found that a Cik1p-GAL4 DNA-binding domain fusion [Cik1(20–541)-DBD] strongly interacts with a Kar3p-GAL4 activation-domain fusion [Kar3p(12–514)-AD] when the yeast two-hybrid system is used for detection (Page *et al.*, 1994). Therefore, this method was used to map the region of Cik1p necessary and sufficient to interact with Kar3p, the portion of Kar3p that interacts with these Cik1p regions, and whether either protein can interact with itself. A series of different Cik1-LexA DNA-binding domain fusions and Kar3-Gal4 activation-domain fusions were prepared. Constructs expressing these fusions were transformed into a *lacZ* reporter strain, and interactions were determined by detection of β-galactosidase activity, qualitatively on 5-bromo-4-chloro-3-indolyl-β-D-galactoside (X-Gal) plates (Figure 2) and quantitatively in liquid assays (Table 2).

Cik1p is predicted to form two closely adjacent coiled-coil domains (referred to here as coil I [amino acids 81–203] and coil II [amino acids 219–362]; Figure 2A) separated by a short break in the heptad periodicity. The coiled-coil regions are flanked by putative globular domains at the amino terminus and carboxy terminus. The Cik1-DBD fusions tested contain either most of the protein [Cik1(20–541)], parts of the coiled-coil region alone [Cik1(77–207), Cik1(77–169), Cik1(207–368), and Cik1(218–393)], or varyingly smaller parts of the coiled coil with the amino-terminal domain [Cik1(20–169), Cik1(20–147), Cik1(20–130), and Cik1(20–114); Figure 2A].

All seven of the Cik1p fusions that interact with Kar3p contain significant segments of the Cik1p coiled-coil domain (Figure 2A). Importantly, fusion proteins containing only parts of coil I [Cik1(77–169) and Cik1(115–207)] interact with Kar3p, as do fusions containing only parts of coil II [Cik1(207–368) and Cik1(218–393)]. Thus, either segment of the Cik1p coiled-coil domain is capable of interacting with Kar3p. Two fusions that contain the amino-terminal globular domain and a minimal amount of coil I [Cik1(20–114) and Cik1(20–130)] fail to interact with the full-length Kar3 fusion. These results are identical in a *cik1*Δ two-hybrid reporter strain, demonstrating that endogenous Cik1p does not facilitate the two-hybrid interactions. Thus, the coiled-coil domain is both necessary and sufficient for Cik1p's interaction with Kar3p (Figure 2A).

The Kar3p coiled coil is similar in length to that of Cik1p and has a similar break in heptad periodicity. Because Cik1p interacts with Kar3p along its entire coiled-coil region, we examined whether Cik1p and Kar3p dimerize along their central coiled-coil domains, whether the two proteins assemble in a parallel manner, and whether these interactions are specific from one segment of the coil to another. Constructs expressing *GAL4* activation-domain fusions with the first of

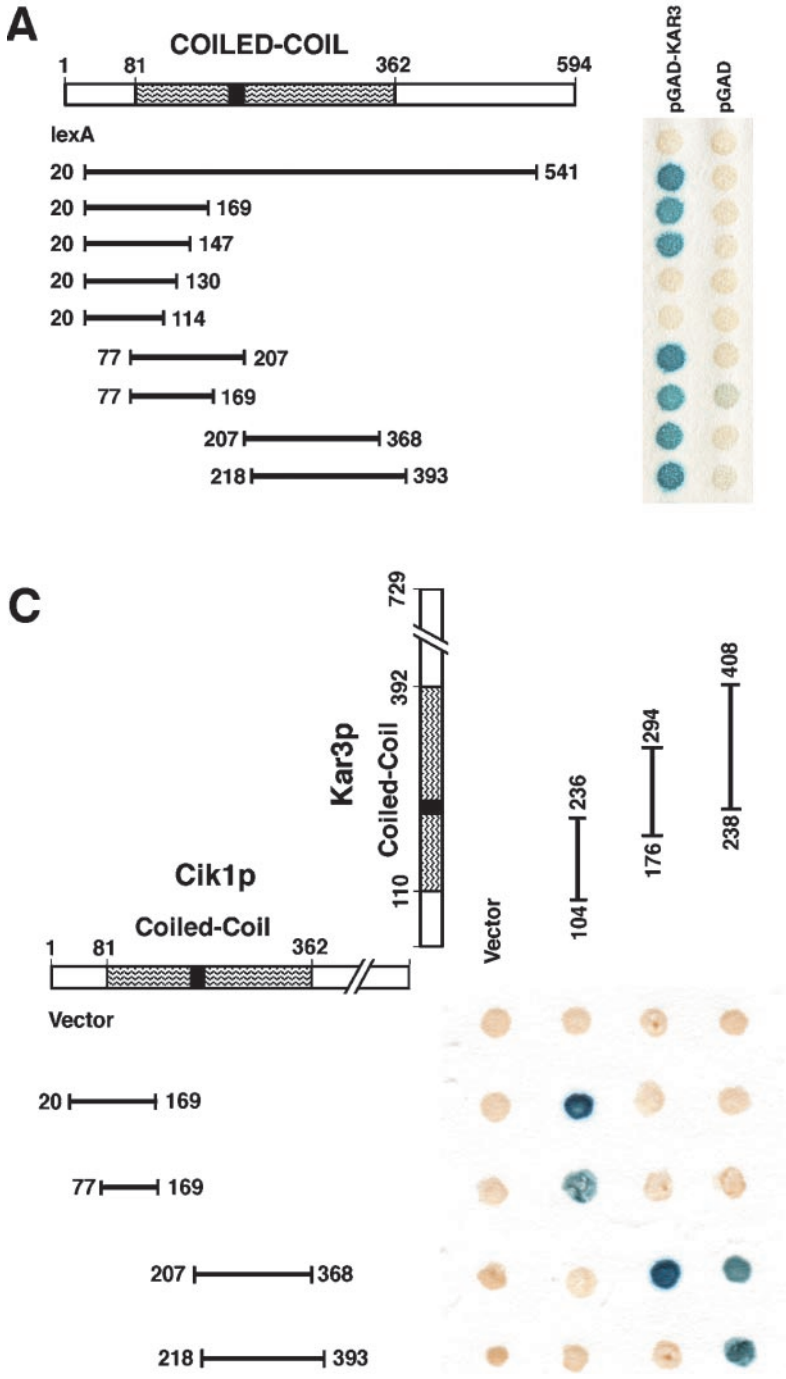

Figure 2. Cik1p and Kar3p associate through specific interactions between their coiled-coil domains. (A) Cik1p interacts with Kar3p through its coiled-coil domain. A scheme of the different Cik1p fusions with the lexA DNA-binding domain is shown, with results of the corresponding two-hybrid experiments shown to the right. Amino acids 81–362 represent the long central coiled coil of Cik1p (predicted coiled-coil domains are indicated by curved lines, with breaks indicated by black boxes). Each construct was tested with both the *KAR3::AD* fusion and with plasmid alone in Y1849. (B) Specificity of the Cik1p-Kar3p interactions. A Cik1p fusion (amino acids 20–541), which interacts with Kar3p, was tested for interaction with full-length Cik1-AD. A Kar3-DBD fusion (amino acids 104–408), which interacts with Cik1p, was tested with full-length Kar3-AD. Cik1-AD and Kar3-AD fusions were also tested for interactions with DBD fusions of the control proteins Kip2p, Spa2p, and NuMA. (C) Kar3p interacts with Cik1p through its coiled-coil domain in a parallel manner. Four of the Cik1-DBD fusions were tested with three Kar3p fusions containing the first half of the Kar3p coiled-coil domain (amino acids 104–236), the middle of the coil (amino acids 176–294) spanning the predicted break (amino acids 237–253), or the second half of the Kar3p coiled-coil domain (amino acids 238–408). In each panel, blue indicates protein-protein interactions resulting in the expression and activity of β-galactosidase, as detected on 5-bromo-4-chloro-3-indolyl-β-D-galactoside (X-Gal)–containing agar plates.

Table 2. Relative β-galactosidase activity of two-hybrid interactions

lexA-DBD fusion	GAL4-AD fusion	Relative β-galactosidase activity[a]
Vector	Vector	1.0
Vector	Cik1(1–594)[b]	0.5
Vector	Kar3(12–514)	0.5
Vector	Kar3(104–236)	1.7
Vector	Kar3(176–294)	1.5
Vector	Kar3(238–408)	1.1
Cik1(20–541)	Vector	0.5
Cik1(20–541)	Cik1(1–594)	0.9
Cik1(20–541)	Kar3(12–514)	34.1
Cik1(20–541)	Kar3(104–236)	26.8
Cik1(20–169)	Vector	0.7
Cik1(20–169)	Cik1(1–594)	0.8
Cik1(20–169)	Kar3(12–514)	85.4
Cik1(20–169)	Kar3(104–236)	23.7
Cik1(20–169)	Kar3(176–294)	1.9
Cik1(20–169)	Kar3(238–408)	1.2
Cik1(20–147)	Vector	1.1
Cik1(20–147)	Kar3(12–514)	51.2
Cik1(20–130)	Vector	1.0
Cik1(20–130)	Kar3(12–514)	0.8
Cik1(20–114)	Vector	0.9
Cik1(20–114)	Kar3(12–514)	0.8
Cik1(77–207)	Vector	0.7
Cik1(77–207)	Kar3(12–514)	37.8
Cik1(77–169)	Vector	1.1
Cik1(77–169)	Kar3(12–514)	19.0
Cik1(77–169)	Kar3(104–236)	92.7
Cik1(77–169)	Kar3(176–294)	21.2
Cik1(77–169)	Kar3(238–408)	17.3
Cik1(207–368)	Vector	0.8
Cik1(207–368)	Kar3(12–514)	63.4
Cik1(207–368)	Kar3(104–236)	2.2
Cik1(207–368)	Kar3(176–294)	24.4
Cik1(207–368)	Kar3(238–408)	212.2
Cik1(218–393)	Vector	0.7
Cik1(218–393)	Kar3(12–514)	14.6
Cik1(218–393)	Kar3(104–236)	0.6
Cik1(218–393)	Kar3(176–294)	0.9
Cik1(218–393)	Kar3(238–408)	34.1

[a] These values are relative to those measured for the vector-vector interaction, which was normalized to a value of 1.0, and were averaged from two experiments.

[b] Numbers in parentheses represent positions within the primary amino acid sequences of Cik1p and Kar3p encoded by each construct.

the Kar3p coiled-coil regions [Kar3(104–236)], with a central region containing the break and parts of both coils [Kar3(176–294)], or with the second coil [Kar3(238–408)] were introduced into strains containing four different Cik1 coiled-coil domain fusions with the LexA-DBD (Figure 2C).

We found that Cik1p and Kar3p interact in a highly specific manner through their coiled-coil domains. Cik1p coil I–containing constructs [Cik1(20–169) and Cik1(77–169)] interact strongly with the first coil of Kar3p [Kar3(104–236)] but do not interact with the Kar3p central coil region [Kar3(176–294)] or the second coil [Kar3(238–408)]. Likewise, Cik1p coil II–containing constructs [Cik1(207–368) and Cik1(218–393)] interact with the Kar3p central coil region and the second coil but not with the first coil of Kar3p (Figure 2C). These results indicate a specific interaction between the amino-terminal portions of the Cik1p and Kar3p coiled-coil domains and, likewise, between the carboxy-terminal halves of the Cik1p and Kar3p coiled-coil domains. These interactions appear to be highly specific between different regions of the two proteins' coiled-coil domains. For instance, Kar3(176–294), which contains the central region of the Kar3p coiled-coil domain, is able to interact only with Cik1(207–368), which contains the more central region of the Cik1p coiled coil (Figure 2C), and does not interact with Cik1(218–393), which is only 11 amino acids shorter at its amino terminus (Figure 2C; Table 2). Together, these data suggest that Cik1p and Kar3p assemble in a parallel manner through specific interactions along the lengths of their respective coiled-coil domains.

A correlation between plate and liquid assays of β-galactosidase activities is seen for each pair of interactions tested except for Cik1(77–169) with Kar3(238–408). These constructs do not give a detectable interaction on plate assays (Figure 2C), but a significant interaction can be detected in liquid assays (Table 2). This discrepancy could be due to nonspecific coiled-coil interactions between these two regions and/or differences in the sensitivity of these two assays.

We also tested if Cik1p interacts with Cik1p, and if Kar3p interacts with Kar3p, by two-hybrid analysis. A construct encoding a full-length Cik1-GAL4 activation-domain fusion (Cik1-AD) was transformed into strains containing vector alone or plasmids encoding Cik1(20–541)-DBD, Cik1(20–169)-DBD, Kar3(104–408)-DBD, or Kar3(104–236)-DBD fusion proteins. Neither Cik1-DBD fusion interacts with Cik1-AD (Figure 2B), whereas they do interact with Kar3-AD (Figure 2A). Cik1-AD also interacts very strongly with Kar3-DBD (Figure 2B). Thus, interaction-competent fusion proteins of Cik1p do not interact with each other in the two-hybrid system. Two Kar3-DBD fusions, one containing the entire coiled-coil domain [Kar3(104–408)] and the other containing the first of the coiled-coil regions [Kar3(104–236); full-length Kar3-DBD self-activated], were also tested for interaction with Kar3-AD. Neither construct interacts with Kar3-AD, whereas both interact with the Cik1-AD fusion (Figure 2B). Thus, although Cik1p and Kar3p interact along the entire lengths of their coiled-coil domains, neither protein appears to use these domains for homodimerization.

To ensure that the Cik1p and Kar3p interaction is specific, the Cik1p and Kar3p fusion proteins were also tested for interaction with other proteins, some of which contain coiled-coil domains. The yeast kinesin-related protein Kip2 contains a long central coiled-coil domain and, when fused with the Gal4 DNA-binding domain, does not interact with Cik1-AD or Kar3-AD fusions in the two-hybrid system (Figure 2B). Likewise, two other coiled-coil–containing proteins, Spa2p and human NuMA, fused to the Gal4 DNA-binding domain do not interact with Cik1-AD or Kar3-AD (Figure 2B). Therefore, the interaction of Cik1p and Kar3p occurs through a highly specific interaction of their coiled-coil domains.

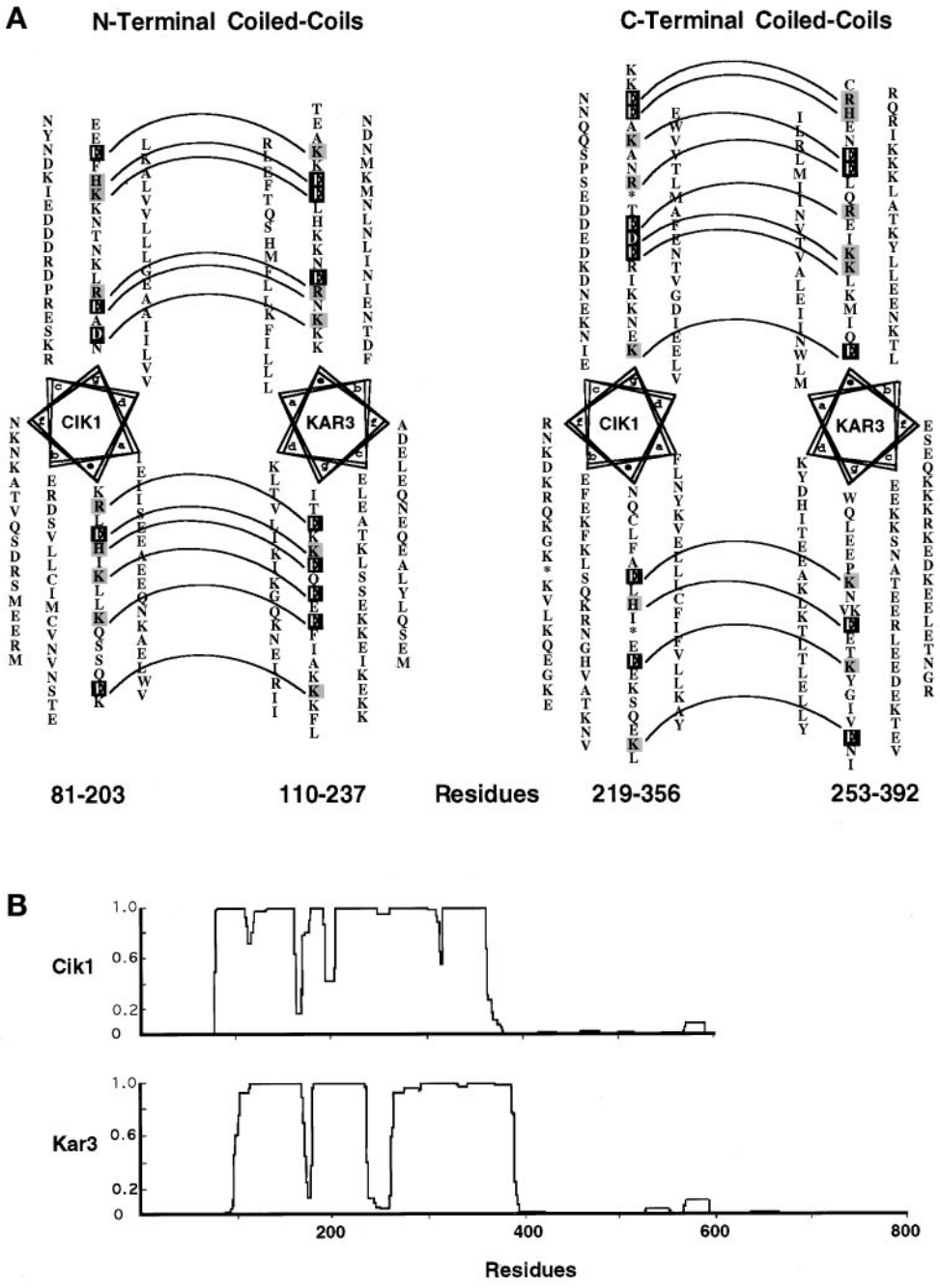

Figure 3. Helical wheel alignments of the coiled-coil domains of Cik1p and Kar3p. (A) Sequence analysis shows how interactions between residues of opposite charges at the *e* and *g* positions in the predicted amino-terminal coiled coils of Cik1p and Kar3p (left) and the predicted carboxy-terminal coiled coils of Cik1p and Kar3p (right) might direct the specific interaction between the proteins' coils. Helical wheels were constructed to represent the heptad periodicity of the predicted coils and are arranged so that the hydrophobic *a* and *d* residues from each of the coils are across from each other. This allows comparison between the *e* and *g* residues of the two proteins that could form electrostatic interactions. When opposite charged residues are present, they are denoted by gray shading (for positively charged) and black shading (for negatively charged), and the pairs are linked by dashed lines. The phase of the heptad repeats was changed at amino acids 293 and 300 for Cik1p and is denoted by asterisks. The phase of the Kar3p repeats was changed once at amino acid 316 and is denoted by having two amino acids in the *g* position. (B) The predicted coiled coils from Cik1p (top) and Kar3p (bottom) are presented with the use of COILS (version 2.2; Lupas, 1996).

Sequence Analysis of the Cik1p and Kar3p Coiled-Coil Domains Might Explain the Specificity and Strength of Their Interactions

To analyze how the Cik1p and Kar3p coiled-coil domains might assemble, helical wheel arrangements of each protein's two coiled-coil regions were generated and compared as described previously for other coiled-coil–containing proteins (e.g., Vinson and Garcia, 1992; Lovejoy *et al.*, 1993) (Figure 3). The Cik1p and Kar3p predicted coiled-coil domains are approximately the same length; for Cik1p, coil I is 122 amino acids and coil II is 137 amino acids; for Kar3p, coil I is 127 amino acids and coil II is 139 amino acids (Figure 3). When the sequences are arranged in a helical wheel such that hydrophobic *a* and *d* residues face each other (*a-g* denotes position within each heptad of the α-helical coiled coil), it is possible to identify residues of opposite charge at the *e* and *g* positions that could form electrostatic interactions within the coiled coil formed between the two proteins. Such interactions have been demonstrated to be important for stabilizing heterodimeric coiled coils (Arndt *et al.*, 2000).

Figure 3A highlights the corresponding *e* and *g* residues from the interacting coils when they are of opposite charge. In the coil I regions of Cik1p and Kar3p, there are 12 possible attractive charge-charge interactions between residues in the *e* and *g* positions and only 3 that are repulsive. In the coil II regions, there are 11 possible attractive interactions between these residues and only 3 possible repulsive interactions. Other alignments were attempted, but this arrangement gave the highest number of possible electrostatic interactions. Alignments between coil I and coil II of the two proteins, or homodimeric coiled-coil alignments, do not predict such a high number of attractive interactions and such a low number of repulsions. These model alignments also agree with the two-hybrid data demonstrating interactions specifically between the amino-terminal coils (coil I) and the carboxy-terminal coils (coil II) within the Kar3p-Cik1p complex.

Cik1p and Kar3p Cofractionate in Sucrose Gradient Density Centrifugation with an Average S Value of 6.26S

To further analyze the nature of the Kar3p-Cik1p complex, sucrose gradient velocity centrifugation and gel filtration experiments were performed with the use of cell lysates prepared from pheromone-treated cells of wild-type *KAR3::HAT*, *cik1*Δ *KAR3::HAT*, or *kar3*Δ strains. Proteins of known sedimentation value and molecular mass were used as standards and were added to each lysate before centrifugation. Proteins from fractions were separated by SDS-PAGE and analyzed by immunoblotting with anti-Cik1p or anti-HA antibodies to follow the proteins of interest. Representative results from three different experiments are shown (Figure 4A).

Wild-type pheromone-treated cell extracts were fractionated via sucrose gradient velocity centrifugation. Under our conditions, a large amount of the Cik1p and Kar3-HAT proteins pellet (see DISCUSSION), whereas the rest is detected sedimenting between aldolase (7.35S) and BSA (4.4S) (Figure 4A). Kar3-HATp exhibits a narrow peak and has an average S value of 6.26 ± 0.2S. Cik1p exhibits a broader sedimentation profile than Kar3-HATp and is present in two peaks. The faster-sedimenting Cik1 protein cofractionates with Kar3-HATp (6.24S), whereas the slower species cofractionates with BSA. These results are consistent with Cik1p and Kar3-HATp associating to form a 6.26S complex with a population of monomeric Cik1p present (4.4S).

Altered Sedimentation Properties of Cik1p and Kar3p from kar3Δ and cik1Δ Cell Lysates

To further analyze the nature of the Kar3p-Cik1p 6.26S complex, the sedimentation behaviors of Cik1p and Kar3-HATp were analyzed in the absence of their respective binding partners. Representative results from three different sets of experiments are shown (Figure 4, B and C); average S values were calculated from the results of all experiments. In *kar3*Δ cell lysates, Cik1p fractionates as a sharper peak, with nearly the same average sedimentation value as BSA (4.3S) and the putative monomeric Cik1p pool from wild-type extracts (Figure 4B). Likewise, a marked difference is seen in the sedimentation pattern of Kar3-HATp in the absence of Cik1p. In *cik1*Δ cell lysates, Kar3-HATp fraction-

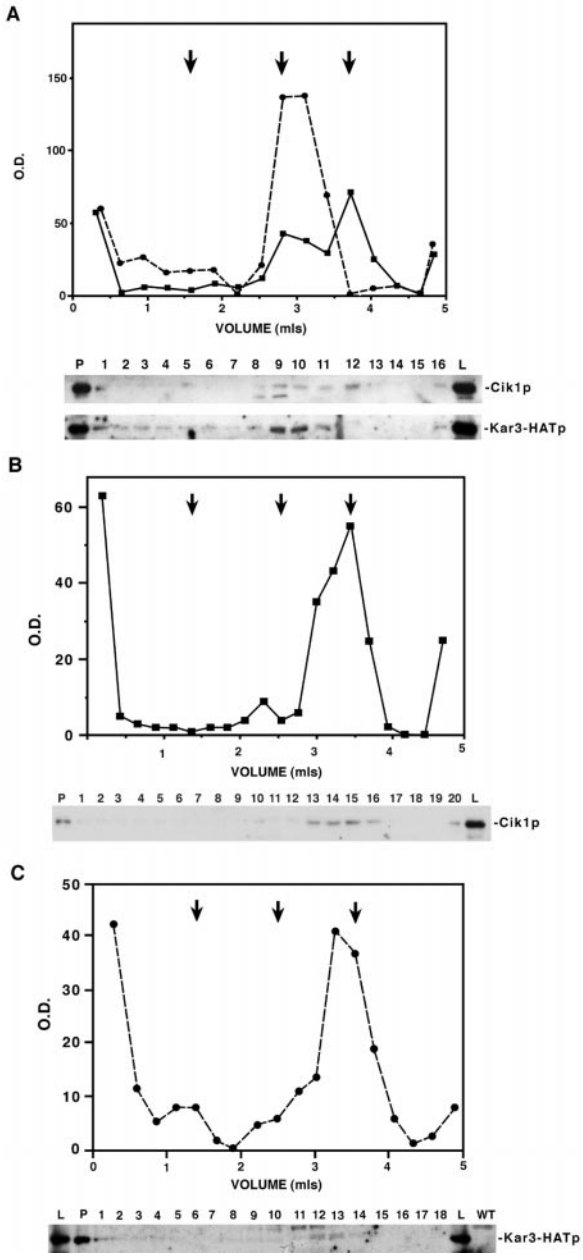

Figure 4. Cik1p and Kar3-HATp cosediment during sucrose density gradient centrifugation with an average S value of 6.26S. Lysates of pheromone-treated cells from wild-type *KAR3::HAT* (Y1870; A), *kar3*Δ (Y1700; B), and *cik1*Δ *KAR3::HAT* (Y1874; C) strains were separated on 5–20% sucrose gradients. Pellets (P), lysates (L), and proteins from collected fractions (fraction numbers) were analyzed by SDS-PAGE and immunoblots with anti-Cik1p antibodies (A, top blot, and B) and anti-HA antibody (A, bottom blot, and C). Proteins present on immunoblots were quantified with the use of NIH Image software (version 1.59) to determine the relative optical density of the protein of interest in each lane. This value is pictured plotted against the volume eluted: Kar3-HATp (dashed line); Cik1p (solid line). Marker proteins of known S values were run simultaneously with the lysates, and the peaks at which they eluted are represented by arrows: catalase (11.3S; left arrows), aldolase (7.4S; middle arrows), and BSA (4.4S; right arrows).

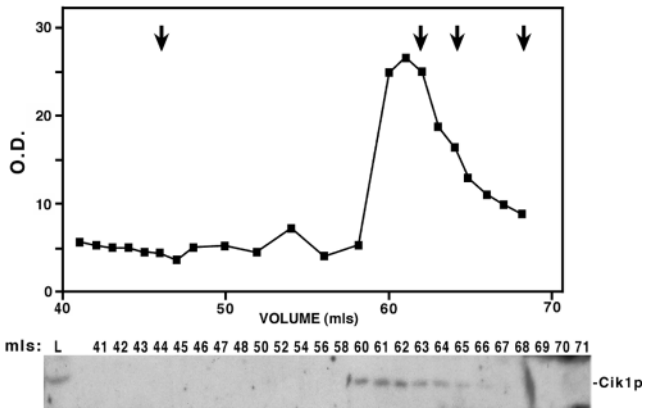

Figure 5. Gel filtration of the Kar3p-Cik1p complex. Peak sucrose gradient fractions in which Kar3p and Cik1p cofractionated (fractions 9, 10, and 11 from Figure 4A) were pooled and run with protein standards on a Sephacryl S-300 gel filtration column with the use of FPLC. The presence of the Kar3-HATp-Cik1p complex in lysates (L) and collected fractions (fraction numbers) was detected on immunoblots with the use of anti-Cik1p antibodies. Cik1 protein present on immunoblots was quantified with the use of NIH Image software (version 1.59) to determine the relative optical density in each fraction. This value is pictured plotted against the volume eluted. The arrows indicate mobilities of standard proteins of known Rs (from left to right): thyroglobulin (8.5 nm), catalase (5.3 nm), aldolase (4.8 nm), and BSA (3.5 nm).

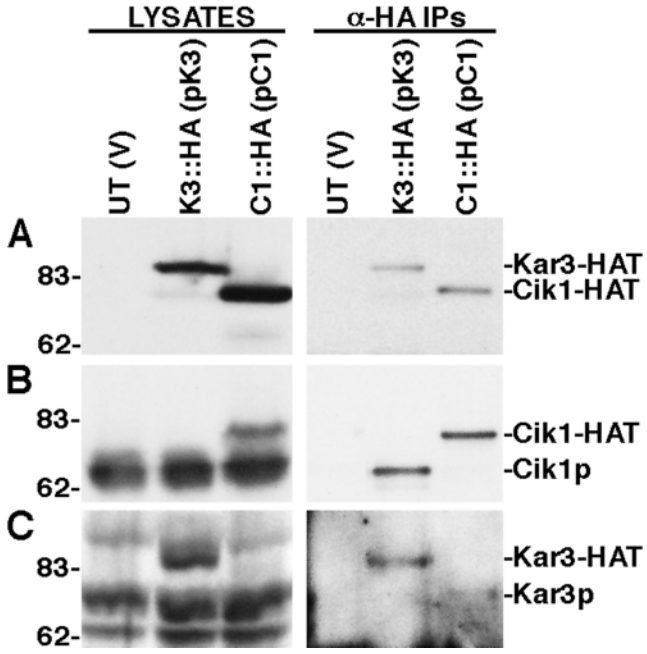

Figure 6. Kar3p and Cik1p associate with each other but not with themselves in immunoprecipitation experiments. Proteins from lysates of α-factor–treated cells from an untagged strain (Y1861) containing a CEN vector (YCp50) alone [UT (V)], a *KAR3::HAT* strain (Y1870) containing YCp50 encoding untagged *KAR3* [K3::HA(pK3)], and a *CIK1::HAT* strain (Y2160) containing a YCp50 encoding untagged *CIK1* [C1::HA(pC1)] were separated by SDS-PAGE and analyzed by immunoblotting (LYSATES) or first immunoprecipitated with anti-HA antibodies (α-HA IPs). These immunoblots were probed with anti-HA antibodies (A), anti-Cik1p antibodies (B), or anti-Kar3p antibodies (C). The identities of the protein bands in both the lysates and immunoprecipitates are denoted on the right, and the positions of molecular mass markers are shown in kilodaltons on the left.

ates in the same region as BSA, with an average predicted S value of 4.6S. This indicates that in the absence of Cik1p, the Kar3-HAT protein behaves as a smaller, presumably monomeric, protein. These data demonstrate that Kar3p and Cik1p interact to form the 6.26S complex.

The Kar3p-Cik1p Complex Has a Molecular Mass of Approximately 148 kDa

The Kar3p-Cik1p complex might be dumbbell-shaped as a result of the long central coiled-coil dimerization domain, and rod-shaped proteins fractionate with S values representative of smaller complexes. Therefore, gel filtration was used to estimate the size of the protein complex. Peak sucrose gradient fractions that contain the major portion of Kar3-HAT were pooled (fractions 9–11), added to a standard set of proteins of known size (thyroglobulin, Rs = 8.5 nm; catalase, Rs = 5.3 nm; aldolase, Rs = 4.8 nm; BSA, Rs = 3.5 nm), and analyzed with the use of FPLC. Because of the small amount of protein used and difficulty in detecting Kar3-HATp, only Cik1p could be detected reliably in the gel filtration fractions by immunoblot analysis. Accordingly, detection of Cik1p was used to determine the Rs of the Kar3-HATp-Cik1p complex from the pooled sucrose gradient fractions in which Kar3p and Cik1p cofractionate.

Cik1p from the Kar3p-Cik1p complex migrated between aldolase and catalase and has a Rs of 5.5 nm (Figure 5). This value and the average S value of 6.26S were used to calculate a predicted molecular mass of 148 kDa (see MATERIALS AND METHODS). Because Kar3-HATp is predicted to be 88 kDa and Cik1p is predicted to be 69 kDa, a size of 157 kDa would be predicted for a 1:1 heterodimer. This value is close to the 148 kDa calculated by sucrose gradient and gel filtration experiments, indicating that Kar3p and Cik1p are likely to form a heterodimer.

To address whether the 4.4S Cik1p sucrose gradient peak is monomeric, the fractions containing this slower-sedimenting peak were pooled and run on the gel filtration column as described for the Kar3p-Cik1p peak. Cik1p peaked at nearly the same fraction as BSA, for a Rs of 3.8 nm (our unpublished data). This value, along with the S value of 4.4S, predicts that this sucrose gradient peak represents monomeric Cik1p with a calculated molecular mass of 72 kDa, very close to its predicted molecular mass of 69 kDa based on primary sequence. The presence of monomeric Cik1p in pheromone-treated cells is consistent with immunoblot analyses demonstrating that Cik1p is more abundant than Kar3p in these cells (Figure 6A). Therefore, it is likely that Cik1p exists both as a monomer and in a heterodimeric complex with Kar3p in cells treated with mating pheromone.

Kar3p and Cik1p Do Not Form Homodimers

The two-hybrid interactions and hydrodynamic properties of Kar3p and Cik1p strongly suggest that these proteins

associate to form a heterodimer. To further confirm that there is only one Kar3p subunit and one Cik1p subunit per complex, coimmunoprecipitation experiments with fully functional HA epitope–tagged (see MATERIALS AND METHODS) and untagged versions of Cik1p and Kar3p were performed. An untagged strain containing a CEN vector alone, a *KAR3::HAT* strain containing a CEN plasmid encoding untagged Kar3p, and a *CIK1::HAT* strain containing a CEN plasmid encoding untagged Cik1p were treated with α-factor before preparation of cell lysates and immunoprecipitation with anti-HA antibodies.

In these lysates, the genome-encoded HA-tagged version of Cik1p or Kar3p can be distinguished from the plasmid-encoded untagged version by a size difference of ~10 kDa, detected on immunoblots probed with polyclonal anti-Cik1p (Figure 6B) or anti-Kar3p (Figure 6C) antibodies. From the *KAR3::HAT/KAR3* lysates, anti-HA antibodies immunoprecipitate Kar3-HATp (Figure 6, A and C) and Cik1p (Figure 6B) but not untagged Kar3p (Figure 6C). Likewise, from the *CIK1::HAT/CIK1* lysates, anti-HA antibodies immunoprecipitate Cik1-HATp (Figure 6, A and B) and Kar3p (Figure 6C) but not untagged Cik1p (Figure 6B). Therefore, under conditions in which Kar3p and Cik1p coimmunoprecipitate, neither protein coimmunoprecipitates with itself. These experiments further demonstrate that the Kar3p-Cik1p complex is a heterodimer and that complexes that contain multiple Kar3p or Cik1p subunits are not present.

In Vegetative Cells, the Kar3p-Cik1p Complex Exhibits Similar Properties to the Complex from Pheromone-treated Cells

Previous genetic and cytological studies suggest that Kar3p and Cik1p also function together during vegetative cell growth (Page *et al.*, 1994; Cottingham *et al.*, 1999; Manning *et al.*, 1999); however, direct association has not been reported. This is likely due to the 20-fold lower abundance of both proteins in these cells relative to pheromone-treated cells and the low titer of the available anti-Kar3p antibodies. To directly demonstrate that Kar3p and Cik1p are also in a complex during the vegetative cell cycle, these proteins were immunoprecipitated from a *KAR3-HAT* strain. The Kar3-HAT protein is detected in lysates and anti-HA immunoprecipitations from both a wild-type and a *cik1*Δ strain but not from a *KAR3* untagged strain (Figure 7). Importantly, Kar3-HATp is also detected in anti-Cik1p immunoprecipitations from the wild-type *KAR3-HAT* strain but not from the *cik1*Δ *KAR3-HAT* strain. This indicates that Cik1p and Kar3p also form a complex in vegetatively growing cells.

The size of the Kar3p-Cik1p complex during vegetative growth was also analyzed. Because of the much lower levels of Cik1p and Kar3p in these cells, and despite significant efforts to analyze the presence of Kar3-HATp, only the presence of the Cik1 protein could be easily monitored. Sucrose gradient velocity sedimentation with lysates from vegetatively growing cells reveals that Cik1p migrates as a single peak and cosediments with aldolase, yielding an S value of 7.3S (Figure 8A). When these peak fractions are run on a gel filtration column, the Cik1 protein peaks with a Rs of 5.4 nm (Figure 8C). Together, these two values calculate a predicted molecular mass of 169 kDa. This agrees with the molecular mass of a Kar3p-Cik1p heterodimer predicted from primary

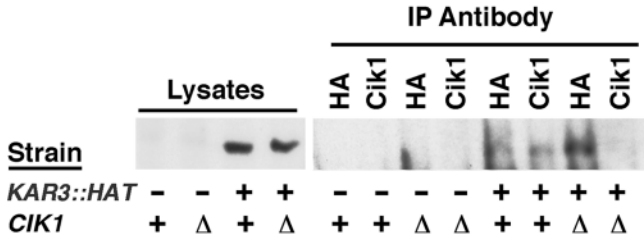

Figure 7. Kar3-HATp coimmunoprecipitates with Cik1p in vegetatively growing cells. Proteins from lysates of vegetatively growing cells from either untagged strains (wild type [Y1861] and *cik1*Δ [Y1850]) or *KAR3::HAT* strains (wild type [Y1870] and *cik1*Δ [Y1874]) were separated by SDS-PAGE and analyzed by immunoblotting (Lysates) or first immunoprecipitated with anti-HA or anti-Cik1p antibodies (IP Antibody). The genotype of the strain in each lane is denoted under the immunoblot. Immunoblots were probed with anti-HA antibodies.

sequence (157 kDa) and is similar to the molecular mass calculated from pheromone-treated cells (148 kDa).

To confirm that this population of Cik1p was from the Kar3p-Cik1p complex, Cik1p was analyzed from vegetative *kar3*Δ cell lysates by sucrose gradient centrifugation. In the absence of Kar3p, the Cik1 protein peaked in the same fraction as BSA, for an S value of 4.4S (Figure 8B), as seen for monomeric Cik1p from pheromone-treated cells. The absence of a monomeric pool of Cik1p in wild-type vegetative cell lysates is consistent with immunoblot analyses demonstrating that, unlike in pheromone-treated cells, Kar3p is more abundant than Cik1p in vegetatively growing cells (B.D. Manning, unpublished result). These data demonstrate that during the vegetative cell cycle all of the Cik1p is associated with Kar3p in a heterodimeric complex.

DISCUSSION

The Kar3p-Cik1p Complex Is a Heterodimer Associated Through a Long Coiled-Coil Stalk Domain

We used several different approaches to demonstrate that Kar3p and Cik1p assemble into a highly stable complex through specific parallel interactions along the entire lengths of their coiled-coil domains. Detailed two-hybrid analyses indicated that the coiled-coil interactions between Kar3p and Cik1p are highly specific and that neither protein interacts with itself or with other coiled-coil proteins tested. Therefore, unlike previously characterized kinesin complexes, in which motor subunits use most or all of their coiled-coil domains to interact with other motor subunits (deCuevas *et al.* 1992; reviewed by Vale and Fletterick, 1997; Hirokawa, 1998), Kar3p interacts with a nonmotor subunit, Cik1p, throughout the length of its coiled-coil domain.

The surprising use of Kar3p's dimerization domain to interact with Cik1p rather than itself suggested that the Kar3p-Cik1p complex might have a novel heterodimeric structure. Sucrose gradient, gel filtration, and immunoprecipitation experiments were performed to demonstrate that the Kar3p-Cik1p complex is indeed a heterodimer, consisting of one Kar3 subunit and one Cik1 subunit. The calcu-

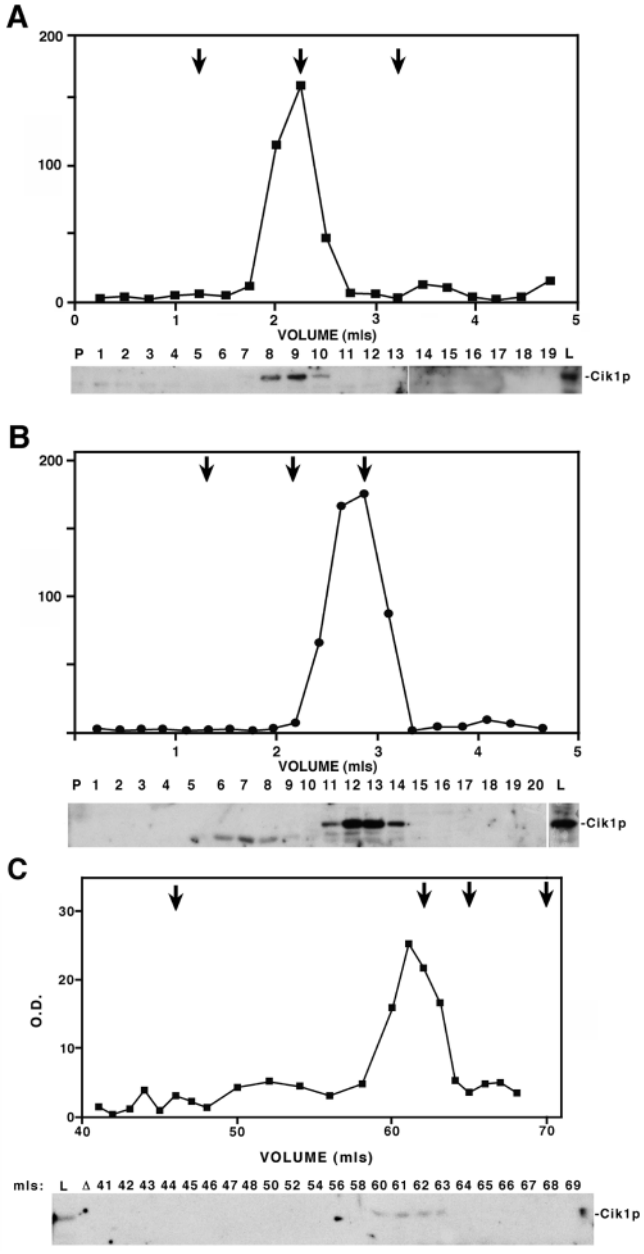

Figure 8. The Kar3p-Cik1p complex has similar size characteristics in vegetatively growing cells to those exhibited in pheromone-treated cells. (A and B) Sucrose density gradient centrifugation was performed on vegetatively growing wild-type *KAR3::HAT* (Y1870; A) and *kar3*Δ (Y1700; B) cell lysates. The Cik1 protein from pellets (P), lysates (L), and collected fractions (fraction numbers) were detected by immunoblots probed with anti-Cik1p antibodies. Cik1p on immunoblots was quantified with the use of NIH Image software (version 1.59) to determine the relative optical density of the protein in each lane. This value is pictured plotted against the volume eluted. Marker proteins of known S values were run simultaneously with the lysates, and the peaks at which they eluted are represented by arrows: catalase (11.3S; left arrows), aldolase (7.4S; middle arrows), and BSA (4.4S; right arrows). (C) Peak Cik1p fractions from the wild-type sucrose gradient experiment (fractions 8, 9, and 10 in A) were pooled and fractionated on a Sephacryl S-300 gel filtration column with the use of FPLC. Cik1p from collected fractions was analyzed on anti-Cik1p immunoblots, and the measured relative optical density of the protein in each fraction is shown plotted against the volume eluted. The arrows indicate mobilities of standard proteins of known Rs (from left to right): thyroglobulin (8.5 nm), catalase (5.3 nm), aldolase (4.8 nm), and BSA (3.5 nm).

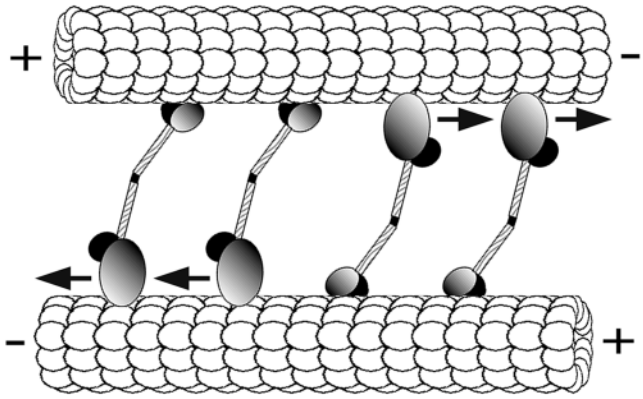

Figure 9. Model of the structure and function of the heterodimeric Kar3p-Cik1p complex in cross-linking and sliding antiparallel microtubules. Kar3p (gray shading) and Cik1p (black shading) interact through an extended coiled-coil stalk domain containing a short break or hinge region. The amino-terminal globular domains of the two proteins (small ovals) act together to bind a microtubule, whereas the motor domain of Kar3p (large ovals with arrows) binds and moves along an antiparallel microtubule toward its minus end. Several Kar3p-Cik1p complexes acting together could pull the minus ends of microtubules toward one another. This activity could drive the nuclear congression step of karyogamy and create the force needed for proper mitotic spindle assembly and/or stability, because both proteins are required for these processes.

lated molecular mass of the complex from these experiments, 148 kDa from pheromone-treated cells and 169 kDa from vegetatively growing cells, is in close agreement with that predicted from the combined primary amino acid sequence of Kar3p and Cik1p, 157 kDa. The smaller 148-kDa complex detected in pheromone-treated cells might reflect the α-factor–induced shift to a faster-migrating form of Cik1p commonly seen by SDS-PAGE and immunoblot analyses (Page and Snyder, 1992; Manning *et al.*, 1999). In the absence of their binding partners, Kar3p and Cik1p behave as smaller monomeric proteins. Together, these molecular genetic and biochemical studies provide strong evidence that the Kar3p-Cik1p complex is a heterodimer (Figure 9) and that neither protein forms homodimeric structures.

To decrease the chances of disrupting native Kar3p-Cik1p complexes, lysates for sucrose gradient experiments were prepared with the use of relatively low salt concentrations (140 mM NaCl). Under these conditions, a large portion of Kar3p and Cik1p is detected in pellets of sucrose gradients from lysates of pheromone-treated cells but not from vegetatively growing cells. The nature of this insoluble fraction of Kar3p and Cik1p, which is specific to pheromone-treated cells, is currently unknown. However, an increase in Kar3p

and Cik1p solubility is observed when cell lysates are treated with higher concentrations of salt or urea (B.D. Manning, unpublished observations).

Conventional KHC and KLC are known to interact through short regions of coiled coil (Gauger and Goldstein, 1993; Diefenbach *et al.*, 1998; Verhey *et al.*, 1998), but to date no KRP has been shown to possess an extensive dimerization domain with a nonmotor protein. The majority of KRPs identified thus far are predicted to contain regions with a propensity to form coiled-coil interactions (Vale and Fletterick, 1997; Hirokawa, 1998). It has been postulated that these regions associate, at least in part, with other motor subunits to form oligomeric complexes with two or more motor domains. Our finding that Kar3p associates with Cik1p through the entire length of its coiled-coil domain raises the interesting possibility that other KRPs might also form such heterodimeric complexes with regulatory proteins.

Implications for Kar3p-Cik1p Function and the Structure of Other Kinesin Complexes

The functional implications of the parallel arrangement of the Kar3p-Cik1p heterodimer may be far-reaching. In this complex, the carboxy-terminal microtubule motor domain of Kar3p might be in close proximity to the carboxy-terminal globular region of Cik1p, raising the possibility that Cik1p might play a regulatory role in the microtubule motor activity of Kar3p. Likewise, the amino-terminal globular domains of Cik1p and Kar3p may also be brought into close proximity by the coiled-coil stalk interaction (Figure 9). This possibility is particularly interesting when one considers that the amino-terminal globular domain of Kar3p is likely to possess a microtubule-binding domain, because a Kar3–β-galactosidase fusion protein lacking the motor domain localizes to cytoplasmic microtubules in pheromone-treated cells (Meluh and Rose, 1990). Interestingly, this nonmotor domain microtubule localization is dependent on Cik1p (Page *et al.*, 1994), suggesting that the amino-terminal globular regions of both proteins together might form a functional microtubule-binding domain. The ability to bind microtubules with regions of both the motor domain and the nonmotor domain would be consistent with the requirement for this complex in the nuclear congression step of karyogamy. Mating cells lacking either Kar3p or Cik1p fail to interdigitate their microtubules and pull their nuclei together after cell fusion (Meluh and Rose, 1990; Page *et al.*, 1994), suggesting that this complex normally acts as a microtubule cross-linking and sliding motor (Figure 9). Finally, both Cik1p and Kar3p have recognizable nuclear localization signals in their globular amino-terminal regions. Because this complex functions both in the cytoplasm during mating and within the nucleus during mitosis (Page *et al.*, 1994), the nuclear localization signals in these regions are likely to be important elements in the regulation of compartmentalization of the complex during the yeast life cycle.

The heterodimeric nature of the Kar3p-Cik1p structure indicates that each complex contains a single motor domain. The presence of two motor domains is thought be critical for the processive movement of kinesin complexes along microtubules (Berliner *et al.*, 1995). However, monomeric KRPs have been identified (Nangaku *et al.*, 1994; Okada *et al.*, 1995), and these proteins may be processive (Okada and Hirokawa, 1999). We speculate that the binding of multiple Kar3p-Cik1p complexes along the interdigitated antiparallel microtubules of mating cells or the mitotic spindles of vegetative cells alleviates the need for multiple motor domains within a single complex (Figure 9). Binding of the nonmotor domain to its cargo (i.e., a microtubule) would prevent the motor complex from diffusing away while moving along the microtubule. If similar heterodimeric single-headed kinesin complexes exist, these might also function on large cargo in concert with several identical complexes.

ACKNOWLEDGMENTS

We thank D.G. Cole for technical advice and assistance, N. Fortin for technical assistance, and S. McPhearson for the *NuMA-Gal4-DBD* fusion construct. J.G.B. and B.D.M. were supported by National Institutes of Health (NIH) training grants and NIH grants GM36494 and GM52197. This research was funded by NIH grants GM36494 and GM52197.

REFERENCES

Arndt, K., Pelletier, J., Muller, K., Alber, T., Michnick, S., and Pluckthun, A. (2000). A heterodimeric coiled-coil peptide pair selected *in vivo* from a designed library-*versus*-library ensemble. J. Mol. Biol. *295*, 627–639.

Berliner, E., Young, E., Anderson, K., Mahtani, H., and Gelles, J. (1995). Failure of single-headed kinesin to track parallel to microtubule protofilaments. Nature *373*, 718–721.

Bloom, G.S., Wagner, M.C., Pfister, K.K., and Brady, S.T. (1988). Native structure and physical properties of bovine brain kinesin and identification of the ATP-binding subunit polypeptide. Biochemistry *27*, 3409–3416.

Brady, S. (1985). A novel brain ATPase with properties expected for the fast axonal transport motor. Nature *317*, 73–75.

Brent, R., and Ptashne, M. (1985). A eukaryotic transcriptional activator bearing the DNA specificity of a prokaryotic repressor. Cell *43*, 729–736.

Cantor, C., and Schimmel, P. (1980). Biophysical Chemistry. Part II. Techniques for the Study of Biological Structure and Function. San Francisco: W.H. Freeman and Company, 846.

Chen, D.C., Yang, B.C., and Kuo, T.T. (1992). One-step transformation of yeast in stationary phase. Curr. Genet. *21*, 83–84.

Cole, D., Saxton, W., Sheehan, K., and Scholey, J. (1994). A slow homotetrameric kinesin-related motor protein purified from *Drosophila* embryos. J. Biol. Chem. *269*, 22913–22916.

Cole, D.G., Chinn, S.W., Wedaman, K.P., Hall, K., Vuong, T., and Scholey, J.M. (1993). Novel heterotrimeric kinesin-related protein purified form sea urchin eggs. Nature *366*, 268–270.

Cottingham, F., Gheber, L., Miller, D., and Hoyt, M. (1999). Novel roles for *Saccharomyces cerevisiae* mitotic spindle motors. J. Cell Biol. *147*, 335–349.

Coy, D., Hancock, W., Wagenbach, M., and Howard, J. (1999). Kinesin's tail domain is an inhibitory regulator of the motor domain. Nat. Cell Biol. *1*, 288–292.

deCuevas, M., Tao, T., and Goldstein, L. (1992). Evidence that the stalk of *Drosophila* kinesin heavy chain is an a-helical coiled coil. J. Cell Biol. *116*, 957–965.

Desai, A., Verma, S., Mitchison, T., and Walczak, C. (1999). Kin I kinesins are microtubule-destabilizing enzymes. Cell *96*, 69–78.

Diefenbach, R., Mackay, J., Armati, P., and Cunningham, A. (1998). The C-terminal region of the stalk domain of ubiquitous human

kinesin heavy chain contains the binding site for kinesin light chain. Biochemistry *37*, 16663–16670.

Endow, S.A., Kang, S.J., Satterwhite, L.L., Rose, M.D., Skeen, V.P., and Salmon, E.D. (1994). Yeast Kar3 is a minus-end microtubule motor protein that destabilizes microtubules preferentially at the minus ends. EMBO J. *13*, 2708–2713.

Friedman, D., and Vale, R. (1999). Single-molecule analysis of kinesin motility reveals regulation by the cargo-binding tail domain. Nat. Cell Biol. *1*, 293–297.

Gauger, A.K., and Goldstein, L.S.B. (1993). The *Drosophila* kinesin light chain. J. Biol. Chem. *268*, 13657–13666.

Goldstein, L., and Philip, A. (1999). The road less traveled: emerging principles of kinesin motor utilization. Annu. Rev. Cell Dev. Biol. *15*, 141–183.

Gordon, D., and Roof, D. (1999). The kinesin-related protein Kip1p of *Saccharomyces cerevisiae* is bipolar. J. Biol. Chem. *274*, 28779–28786.

Hackney, D.D., Levitt, J.D., and Suhan, J. (1992). Kinesin undergoes a 9 S to 6 S conformation transition. J. Biol. Chem. *267*, 8696–8701.

Hirokawa, N. (1998). Kinesin and dynein superfamily proteins and the mechanism of organelle transport. Science *279*, 519–526.

Ito, H., Fukada, Y., Murata, K., and Kimura, A. (1983). Transformation of intact yeast cells with alkali cations. J. Bacteriol. *153*, 163–168.

Kashina, A., Baskin, R., Cole, D., Wedaman, K., Saxton, W., and Scholey, J. (1996). A bipolar kinesin. Nature *379*, 270–272.

Kuznetsov, S., Vaisberg, Y., Shanina, N., Magretova, N., Chernyak, V., and Gelfand, V. (1988). The quaternary structure of bovine brain kinesin. EMBO J. *7*, 353–356.

Laemmli, U.K. (1970). Cleavage of structural proteins during the assembly of the head of bacteriophage T4. Nature *227*, 680–685.

Lovejoy, B., Choe, S., Cascio, D., McRorie, D., DeGrado, W., and Eisenberg, D. (1993). Crystal structure of a synthetic triple-stranded alpha-helical bundle. Science *259*, 1288–1293.

Lupas, A. (1996). Prediction and analysis of coiled-coil structures. Methods Enzymol. *266*, 513–525.

Manning, B., Barrett, J., Wallace, J., Granok, H., and Snyder, M. (1999). Differential regulation of the Kar3p kinesin-related protein by two associated proteins, Cik1p and Vik1p. J. Cell Biol. *144*, 1219–1233.

McDonald, H., Stewart, R., and Goldstein, L. (1990). The kinesin-like *ncd* protein of *Drosophila* is a minus end-directed microtubule motor. Cell *63*, 1159–1165.

Meluh, P.B., and Rose, M.D. (1990). *KAR3*, a kinesin-related gene required for yeast nuclear fusion. Cell *60*, 1029–1941.

Nangaku, M., Sato-Yoshitake, R., Okada, Y., Noda, Y., Takemura, R., Yamazaki, H., and Hirokawa, N. (1994). KIF1B, a novel microtubule plus end-directed monomeric motor protein for transport of mitochondria. Cell *79*, 1209–1220.

Okada, Y., and Hirokawa, N. (1999). A processive single-headed motor: kinesin superfamily protein KIF1A. Science *283*, 1152–1157.

Okada, Y., Yamazaki, H., Sekine-Aizawa, Y., and Hirokawa, N. (1995). The neuron-specific kinesin superfamily protein KIF1A is a unique monomeric motor for anterograde axonal transport of synaptic vesicle precursors. Cell *81*, 769–780.

Page, B.D., Satterwhite, L.L., Rose, M.D., and Snyder, M. (1994). Localization of the KAR3 kinesin heavy chain-like protein requires the CIK1 interacting protein. J. Cell Biol. *124*, 507–519.

Page, B.D., and Snyder, M. (1992). CIK1: a developmentally regulated spindle pole body-associated protein important for microtubule functions in *Saccharomyces cerevisiae*. Genes Dev. *6*, 1414–1429.

Ross-MacDonald, P., Sheehan, A., Roeder, G.S., and Snyder, M. (1997). A multipurpose transposon system for analyzing protein production, localization, and function in *Saccharomyces cerevisiae*. Proc. Natl. Acad. Sci. USA *94*, 190–195.

Sambrook, J., Fritsch, E.F., and Maniatis, T. (1989). Molecular Cloning: A Laboratory Manual, Cold Spring Harbor, NY: Cold Spring Harbor Laboratory.

Saunders, W., Hornack, D., Lengyel, V., and Deng, C. (1997). The *Saccharomyces cerevisiae* kinesin-related motor Kar3p acts at preanaphase spindle poles to limit the number and length of cytoplasmic microtubules. J. Cell Biol. *137*, 417–431.

Saunders, W., and Hoyt, M.A. (1992). Kinesin-related proteins required for structural integrity of the mitotic spindle. Cell *70*, 451–458.

Scholey, J.M. (1996). Kinesin-II, a membrane traffic motor in axons, axonemes, and spindles. J. Cell Biol. *133*, 1–4.

Scholey, J.M., Heuser, J., Yang, J.T., and Goldstein, L.S.B. (1989). Identification of globular mechanochemical heads of kinesin. Nature *338*, 355–357.

Sherman, F., Fink, G.R., and Hicks, J.B. (1986). Methods in Yeast Genetics, Cold Spring Harbor, NY: Cold Spring Harbor Laboratory.

Sheu, Y., Santos, B., Fortin, N., Costigan, C., and Snyder, M. (1998). Spa2p interacts with cell polarity proteins and signaling components involved in yeast cell morphogenesis. Mol. Cell. Biol. *18*, 4053–4069.

Skoufias, D., Cole, D., Wedaman, K., and Scholey, J. (1994). The carboxyl-terminal domain of kinesin heavy chain is important for membrane binding. J. Biol. Chem. *269*, 1477–1485.

Stenoien, D.L., and Brady, S.T. (1997). Immunochemical analysis of kinesin light chain function. Mol. Biol. Cell *8*, 675–689.

Stock, M., Guerrero, J., Cobb, B., Eggers, C., Huang, T., Li, X., and Hackney, D. (1999). Formation of the compact conformer of kinesin requires a COOH-terminal heavy chain domain and inhibits microtubule-stimulated ATPase activity. J. Biol. Chem. *274*, 14617–14623.

Vale, R.D., and Fletterick, R.J. (1997). The design plan of kinesin motors. Annu. Rev. Cell Dev. Biol. *13*, 745–777.

Vale, R.D., Reese, T.S., and Sheetz, M.P. (1985). Identification of a novel force generating protein, kinesin, involved in microtubule-based motility. Cell *42*, 39–50.

Verhey, K.J., Lizotte, D.L., Abramson, T., Barenboim, L., Schnapp, B.J., and Rapoport, T.A. (1998). Light chain-dependent regulation of kinesin's interaction with microtubules. J. Cell Biol. *143*, 1053–1066.

Vinson, C., and Garcia, K. (1992). Molecular model for DNA recognition by the family of basic-helix-loop-helix-zipper proteins. New Biol. *4*, 396–403.

Wedaman, K.P., Meyer, D.W., Rashid, D.J., Cole, D.G., and Scholey, J.M. (1996). Sequence and submolecular localization of the 115-kD accessory subunit of the heterotrimeric kinesin-II ($KRP_{85/95}$) complex. J. Cell Biol. *132*, 371–380.

Yamazaki, H., Nakata, T., Okada, Y., and Hirokawa, N. (1996). Cloning and characterization of KAP3: a novel kinesin superfamily-associated protein of KIF3A/3B. Proc. Natl. Acad. Sci. USA *93*, 8443–8448.

Yang, J.T., Laymon, R.A., and Goldstein, L.S.B. (1989). A three-domain structure of kinesin heavy chain revealed by DNA sequence and microtubule binding analyses. Cell *56*, 879–889.

Yang, J.T., Saxton, W., Stewart, R., Raff, E., and Goldstein, L.S. (1990). Evidence that the head of kinesin is sufficient for force generation and motility in vitro. Nature *249*, 42–47.